Available online at www.sciencedirect.com
SCIENCE DIRECT®

Journal of the European Ceramic Society 23 (2003) 2351–2360
www.elsevier.com/locate/jeurceramsoc

Role of microstructure in the grinding and polishing of α-sialon ceramics

Zong-Han Xie[a,*], Robert J. Moon[a], Mark Hoffman[a], Paul Munroe[a], Yi-Bing Cheng[b]

[a]*School of Materials Science and Engineering, University of New South Wales, NSW 2052, Australia*
[b]*School of Physics and Materials Engineering, Monash University, VIC 3800, Australia*

Received 10 June 2002; received in revised form 12 December 2002; accepted 5 January 2003

Abstract

The grinding and polishing behaviour of three tailored α-sialon microstructures made of the same chemical composition: fine-grained, bimodal and large elongated-grained, were determined. The fine-grained microstructure was characterised by extensive lateral cracks in the grinding process and widespread grain pullout during the mechanical polishing; in contrast, the large elongated-grained microstructure exhibited high grinding damage resistance, and a defect-free, mirror-like surface after mechanical polishing. The bimodal microstructure showed an intermediate behaviour during both processes. The material removal mechanisms during grinding and polishing were analysed and modelled as a function of grain size and aspect ratio.

Keywords: Focus ion beam (FIB) technique; Grinding; Microstructure; Polishing; Sialons

1. Introduction

The development of in-situ toughened α-sialon ceramics provides ceramic materials with improved fracture toughness.[1,2] A recent processing investigation of a Ca-doped α-sialon composition has developed three varied microstructures; fine grained (EQ), bimodal (E/E) and large elongated-grained (EL) through variations in the sintering schedule.[3] These three microstructures exhibit some significantly different mechanical properties.

Tailorable microstructure and mechanical properties of α-sialon ceramics make it a promising material for industrial applications. A critical step in the fabrication of ceramic components is to produce high quality surfaces without surface/subsurface damage through machining and surface finishing processes.[4] Therefore, it is necessary to understand the effect of grain size and morphology on the material removal mechanisms of α-sialon ceramics in both grinding and polishing processes. Additionally, the study of α-sialon grinding and polishing behaviours, which represent two extreme forms of abrasive wear, i.e. severe and mild wear, may shed light on abrasive wear mechanisms of ceramics, in general.

Grinding can be defined microscopically as a multiple-point multiple-pass two-body abrasive wear process involving the removal of particles which are significantly larger than the grain size. Two controlling material removal mechanisms have been identified in the abrasive wear process; microcracking[5–9] and lateral cracking.[10–12] Both of these mechanisms are influenced by the material microstructure. For the microcracking-dominated mechanism, fine-grained materials, which exhibited larger short-crack toughness,[13,14] have higher resistance to material removal by abrasive wear than coarse-grained materials.[5–9] Conversely, lateral cracking can be suppressed when grain size exceeds a critical size.[15] However, the effect of grain morphology on microcracking and the formation of lateral cracks during grinding has not been addressed quantitatively.

Mechanical polishing can be identified as a mild three-body abrasive wear process. The material removal occurs at a scale of grain- or subgrain size under low load and the action of polishing particles. The general polishing methods for both β-Si_3N_4 and β-sialon ceramics have been developed.[16] However, the influence of microstructure on surface roughness of sialon ceramics

* Corresponding author.
E-mail address: zhxie@materials.unsw.edu.au (Z.-H. Xie).

0955-2219/03/$ - see front matter © 2003 Elsevier Ltd. All rights reserved.
doi:10.1016/S0955-2219(03)00046-3

during polishing has not been investigated. Alternatively, it was found[17] that the surface roughness of alumina at each stage during mechanical polishing of alumina increased with increasing grain size, and that material removal occurred primarily via grain dislodgment. However, the roles of the microstructural variables, such as grain size and aspect ratio, in the polishing process have not been investigated systematically.

The purpose of this present work is to investigate the effect of grain size and aspect ratio on the material removal mechanisms in the grinding and mechanical polishing processes of α-sialon ceramics via observing and analysing the surface/subsurface damage produced during both processes.

2. Experimental procedure

2.1. Materials processing and characterisation

The α-sialon ceramics used in this study were developed and characterised in terms of grain size, morphology and mechanical properties, as described in detail elsewhere.[3] A brief description is given here for clarification.

2.1.1. Material processing

Powders of Si_3N_4 (Grade M11, H. C. Starck, Berlin, Germany), AlN (Grade B, H. C. Starck, Berlin, Germany), and $CaCO_3$ (Ajax Chemicals, Sydney, Australia) were mixed in the following ratio: 56.6 wt.% Si_3N_4, 23.9 wt.% AlN and 19.5 wt.% $CaCO_3$. This powder mixture was ball-milled in isopropanol for 30 h using Si_3N_4 milling media, and dried at 100 °C for 24 h. This dried powder was pulverised and then compacted using cold isostatic pressing (CIP) of 200 MPa. Three α-sialon microstructures were produced by a two-step sintering technique, as seen in Table 1, in a graphite furnace (Model Group 1400 Hot Presses, Thermal Technology Inc., Santa Rose, CA, USA). The diameter of all sintered samples was 25 mm. Nominal chemical composition is $Ca_xSi_{12-(m+n)}Al_{m+n}O_nN_{16-n}$, where $x=m/2$, $m=2.6$, $n=1.3$.

Table 1
Sintering conditions and the resulting Ca α-sialon microstructures

Sample	Identification	Microstructure	Sintering condition
1	EQ	Fine-grained	1550 °C/0.5 h HPed[a] 25 MPa 1600 °C/0.5 h HPed 25 MPa
2	E/E	Bimodal	1550 °C/0.5 h HPed 25 MPa 1700 °C/0.5 h HPed 25 MPa
3	EL	Large elongated	1750 °C/1.0 h Pressureless 1750 °C/1.0 h HPed 25 MPa

[a] Hped→hot-pressed.

2.1.2. Microstructural and mechanical characterisation

The resulting microstructures were observed via field emission scanning electron microscopy (FESEM) (Model Hitachi 4500 II, Hitachi Co., Japan), and microstructural features were quantified using Leica Q500MC Image Analysis System (Leica Cambridge Ltd, Cambridge, UK). Bulk density was determined by a water immersion method as per Australian Standard AS 1774.5-1989. Vickers hardness was measured (Vickers-Amstrongs Ltd., Grayford Kent, UK) in accordance with ASTM Standard E 384, and fracture toughness was tested (Vickers-Amstrongs Ltd.) and calculated based on an indentation technique.[18]

Field emission scanning electron micrographs of the three microstructures, after chemical etching in molten NaOH, are shown in Fig. 1. Microstructural and mechanical characteristics are outlined in Table 2. All the microstructures show similar hardness. The large elongated microstructure has the highest indentation fracture toughness, which can be attributed to enhanced crack bridging by large elongated grains.[19–22]

2.2. Grinding, lapping and polishing procedures

The α-sialon samples were mounted on steel holders, and ground on a surface grinder (Model KGS-250AH, Kent Industrial Co. Ltd, Taiwan, ROC) with a metal-bonded 220-grit peripheral diamond wheel. The width of the dressed wheel was 20 mm, and the diameter was 150 mm. Surface grinding took place under the following conditions: wheel speed of 2850 r.p.m, longitudinal table velocity of 20 m/min., automatic cross feed rate of 5 mm/stroke and downfeed increment rate of 20 μm/pass. At the final machining step, more than 100 passes

Table 2
Ca α-sialon microstructures and their mechanical properties

Sample identification	Average grain diameter (μm)	Average grain length (μm)	Aspect ratio (A_R)	Density (g/cm^3)	H_V (GPa) Load = 98 N	K_R (MPa$\sqrt{m}$)[a] Load = 98 N
EQ	0.35	0.39	1.1	3.19	12.8±0.5	3.7±0.3
E/E-equiaxed grains	0.38	0.49	1.3	3.20	12.2±0.4	6.1±0.4
E/E-elongated grains	0.46	1.93	4.2			
EL	0.70	5.04	7.2	3.21	12.0±0.2	7.5±0.3

[a] Determined by Vickers Indentation technique.[18]

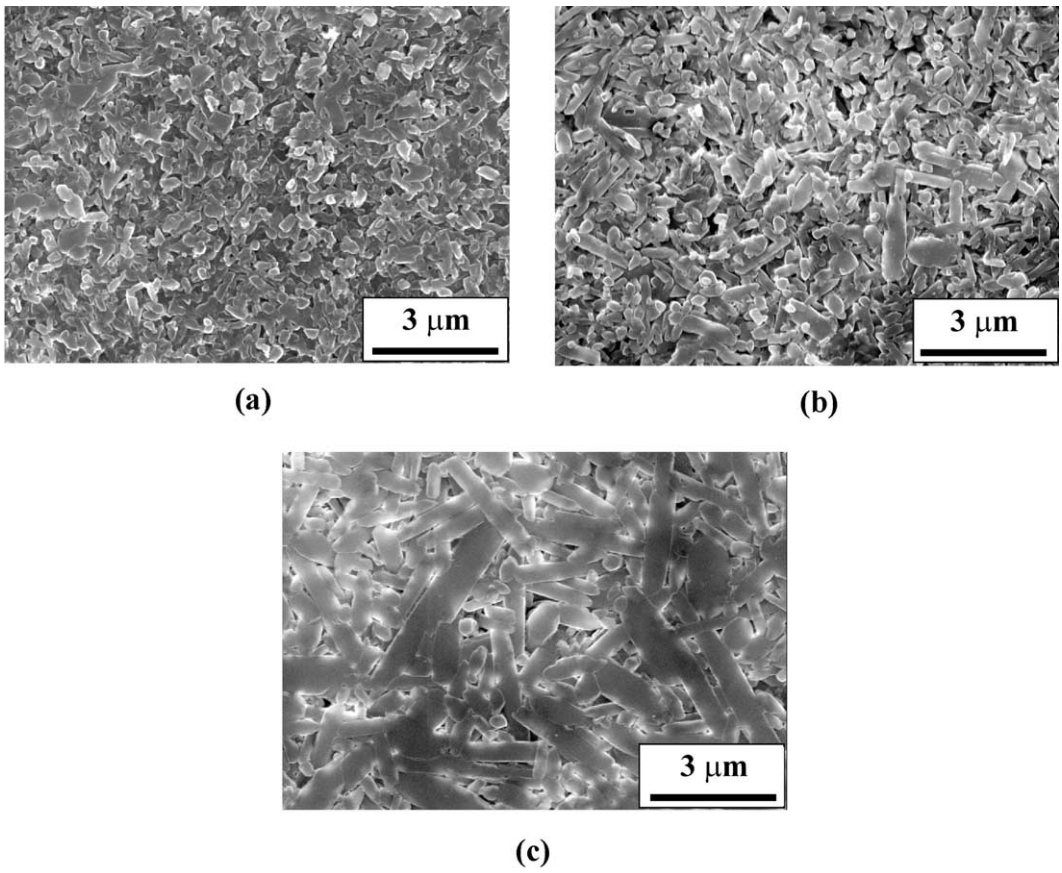

Fig. 1. FESEM micrographs of Ca α-sialon microstructures sintered under different conditions (a) EQ (b) E/E (c) EL.[3]

were used to establish a steady-state condition on the ground surfaces.

After grinding, the samples were ultrasonically cleaned in acetone for 5 min, rinsed with alcohol and then distilled water, and finally dried using high pressure air. The ground surfaces were then lapped (sample holder: LaboForce-3; disc holder: LaboPol-5, Struers, Denmark) with water as lubricant at a fixed feed rate of 1.0 ml/min. The lapping procedure is described in Table 3. After lapping, the same cleaning procedure was applied as that after grinding.

Polishing was performed using the same machine as used for lapping. The procedure is listed in Table 3. The lubricant (Microid diamond compound extender, P/N 811-004, Leco Corporation, USA) was supplied at a fixed rate of 0.8 ml/min. for all polishing steps. The samples were ultrasonically cleaned first with alcohol, then water after each polishing step to eliminate the influence of remnant debris on the subsequent polishing process.

2.3. Surface measurement and subsurface observation techniques

The sample surfaces were first observed via light optical microscopy (Type 090-124.012 Ernst Leitz Wetzlar GMBH, Germany) after grinding, lapping and each polishing step. A surface profilometer (SURFTEST SV-600, Mitutoyo, Japan) with its stylus tip (Diamond, conical 90°, Tip radius 5 μm) normal to the surface was used to measure the surface roughness, Ra, over a trace length of 4 mm. Each of the Ra values was an average of four separate measurements. Measurements were taken both perpendicular and parallel to the original grinding direction.

A focused ion beam (FIB) miller (Focused Ion Beam xP200, FEI Company, Hillsboro, OR 97124 USA) was used to obtain the surface and cross-sectional views of the ground and final polished samples.[23] The miller uses

Table 3
Lapping and polishing procedures for Ca α-sialon

Work process[a]	Abrasive (grit size, μm)	Total time (min)	Load (N)	Speed (rpm)	Polishing Disc[b]
LAP	120	60	40	300	MD Piano120, MANTO
15P	15[c]	45	30	200	MD Allegro, MADTD
6P	6[c]	40	20	150	MD Pan, MAPAN
1P	1[c]	15	10	100	MD Pan, MAPAN

[a] LAP: lapping; 15P, 6P and 1P: mechanical polishing steps.
[b] Producer: Struers, Denmark.
[c] Diamond paste, made by Struers, Denmark.

a fine (~10 nm), energetic beam of gallium ions that scans over the sample surface. At high beam currents the gallium beam rapidly sputters sections through the surface, allowing subsurface cross-sections to be prepared. If the beam current is reduced, the secondary electrons or secondary ions emitted from the sample surface can be detected and used to form high-resolution images, similar to conventional SEM images. This sectioning technique allows micron size features (microcracks etc.), located within ~10 μm of the surface, to be viewed with minimal damage induced during sectioning.

3. Results

3.1. Grinding response

The surface roughness of the three samples after grinding is plotted in Fig. 2 (corresponding to the "G" on the *X*-axis). The small stylus tip fits into the grooves when measuring parallel to the grinding direction, resulting in a significant reduction in surface roughness for all three samples, as compared to the perpendicular direction. EQ exhibited the highest surface roughness in both directions and EL had the lowest.

Optical and focused ion beam (FIB) micrographs of the ground surfaces and subsurfaces, as shown in Fig. 3, reveal distinct features associated with the different microstructures. Grinding grooves and thin deformed layers were present on the ground surfaces of all the samples, however, the extent of surface damage, which was characterised by the size and area fraction of pits, was different among the three microstructures [Fig. 3(a)].

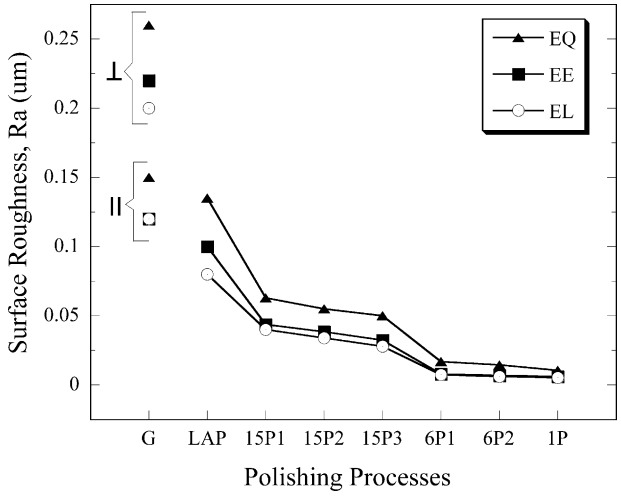

Fig. 2. Surface roughness measured perpendicular (⊥) and parallel (‖) to the grinding direction, and variation of surface roughness as a function of lapping and progressive polishing. G: grinding; LAP, lapping; 15P1, polishing time 15 min; 15P2, polishing time 30 min; 15P3, polishing time 45 min; 6P1, polishing time 20 min; 6P2, polishing time 40 min; 1P, polishing time 15 min.

The ground surface of EQ contained a large number of pits whose size was much larger than the average size of the grains [EQ of Fig. 3(b)]. A cross-sectional view normal to this ground surface reveals lateral and median crack formation beneath the contact surface, in which the lateral cracks have been observed to propagate toward the surface [EQ of Fig. 3(c)], causing the formation of pits. In contrast, on the ground surface of EL well-defined grooves were apparent [EL of Fig. 3(a)]. Extensive grain pullout could be found on the broken surface layer [EL in Fig. 3(b)]. Subsurface microcracking was observed, but lateral and median cracks were not detected [EL of Fig. 3(c)]. The grinding response of E/E showed an intermediate behaviour with the extent of surface damage less than in EQ.

3.2. Lapping response

The surface roughness after lapping is plotted in Fig. 2. In contrast to the ground samples, the measured surface roughness of the lapped samples was reduced and showed no orientation dependence, which is due to continuous variation in the lapping direction. EQ still showed the highest surface roughness after lapping. The surface conditions after lapping are shown in Fig. 4(a). The extent of the surface damage of each sample decreased significantly compared to that after grinding, and EQ still exhibited more damage than both E/E and EL.

3.3. Polishing response

The surface roughness of the three α-sialon samples is plotted against the successive polishing processes in Fig. 2. EQ always showed the highest surface roughness after each polishing step when compared to the other two samples. During polishing with 15 μm diamond paste, EL showed a slightly lower surface roughness than E/E. However, during the subsequent polishing with 6 μm and 1 μm diamond pastes, the surface roughness of EL and E/E tended to the same level.

The polished surfaces of the samples are shown in Fig. 4(b)–(d) after polishing under different diamond pastes. All of the samples exhibited significant improvement of surface quality after the application of 15 μm diamond polishing paste. However, compared to EL and E/E, two types of surface damage still existed on the surface of EQ, even after polishing with 1 μm diamond paste [EQ of Fig. 4(d)]. The first type of damage, which appeared as dark spots ~10 μm in diameter, are pits that remained from the grinding process. The second damage type appeared as bright spots <5 μm in diameter, which are sites of grain pull-out during the polishing process. In a separate test, the grinding damage for EQ was eliminated via extending the lapping time to 3 h. However, the appearance of grain pullout continued even during the prolonged polishing processes.

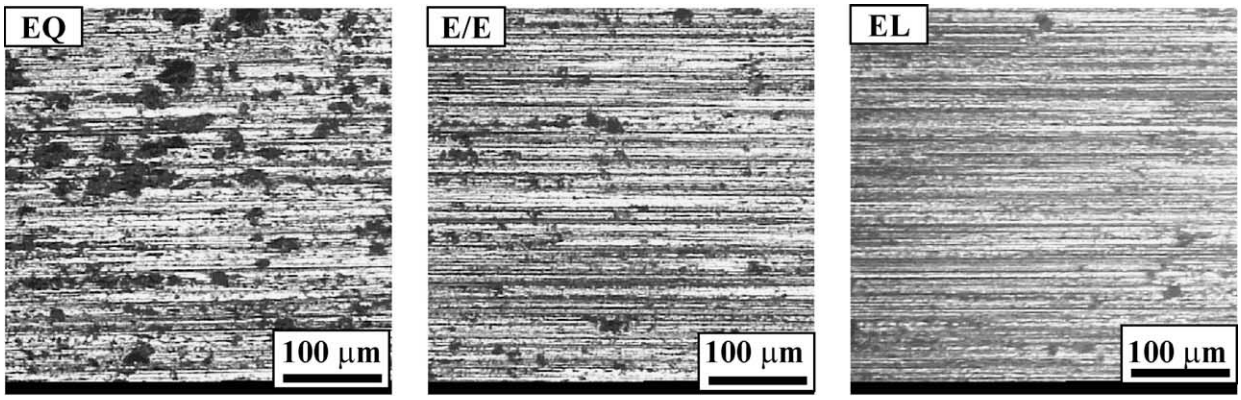

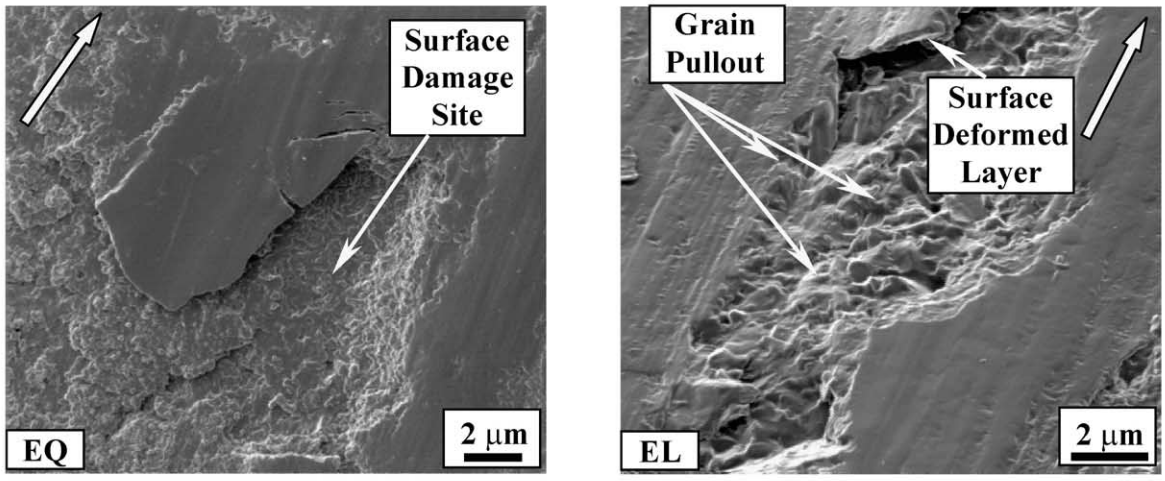

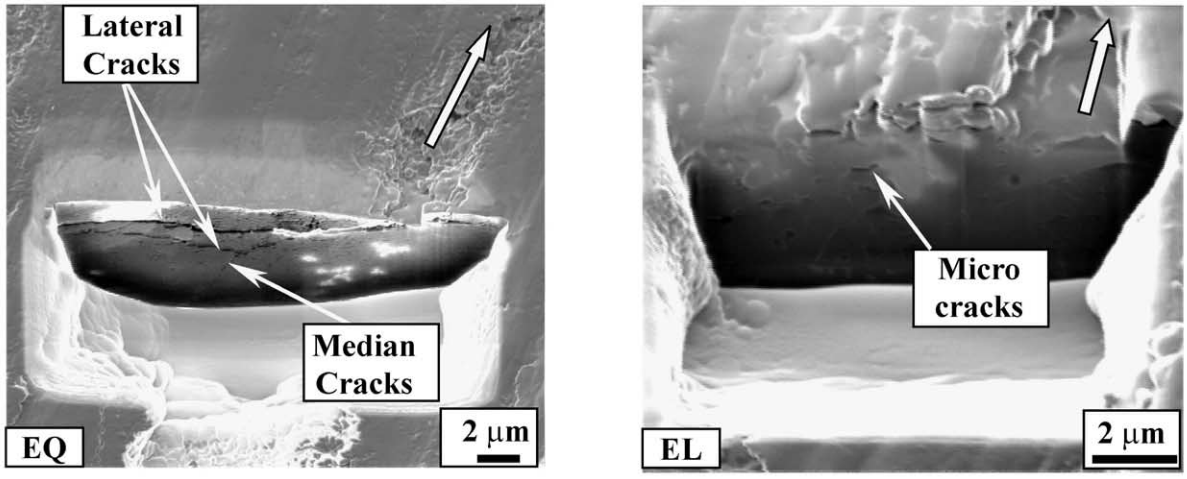

Fig. 3. (a) Optical micrographs of the ground surfaces of EQ, E/E and EL, (b) FIB micrographs of the ground surfaces of EQ and EL, (c) FIB micrographs of subsurface cross-sections (normal to the ground surface) of EQ and EL. The arrows represent the grinding direction.

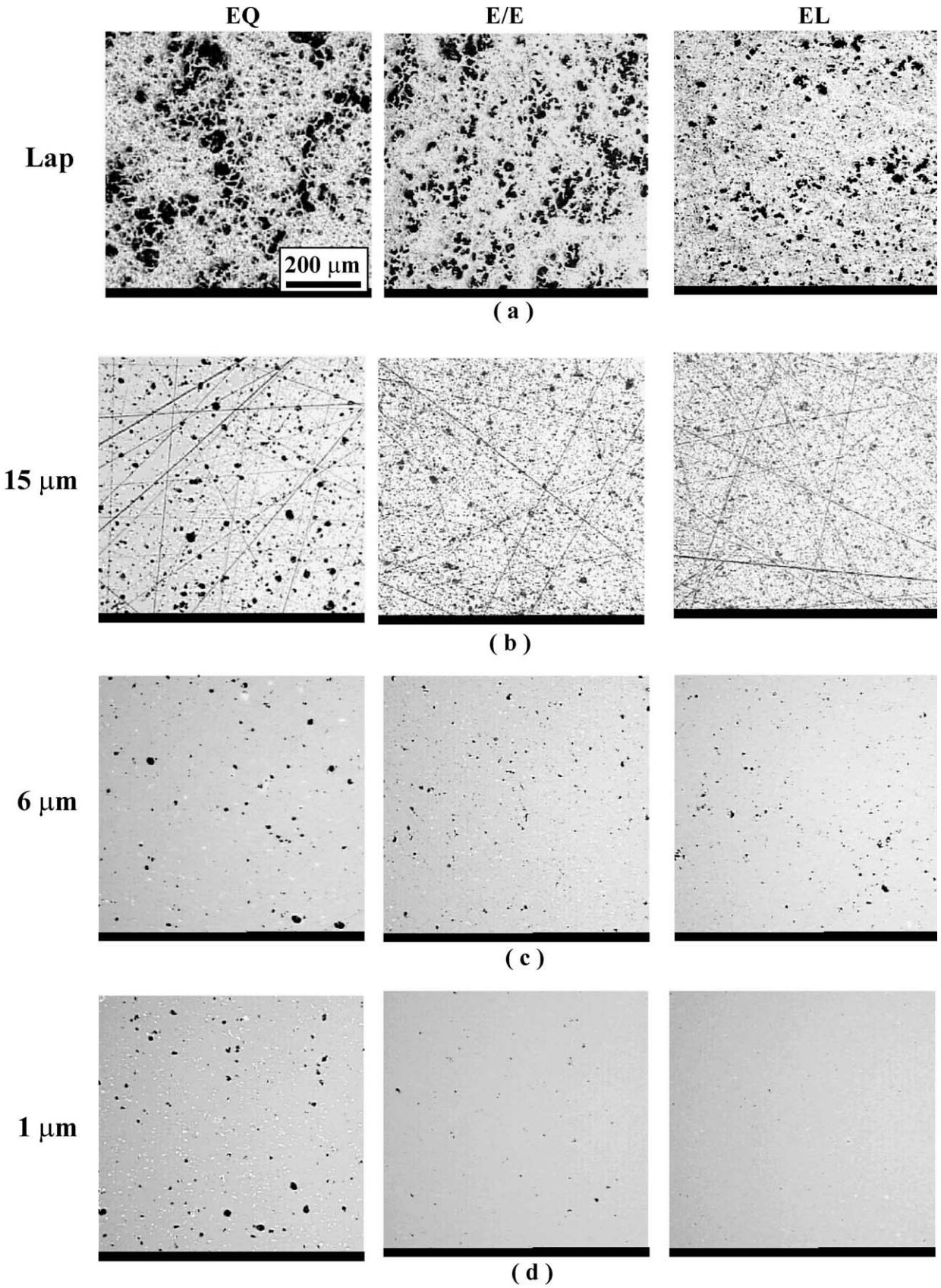

Fig. 4. Surface conditions of EQ, E/E and EL, (a) after lapping for 60 min, (b) after polishing at 15 μm diamond paste for 45 min, (c) after polishing at 6 μm diamond paste for 40 min, (d) after polishing at 1μm diamond paste for 15 min.

4. Discussion

4.1. Effect of microstructure on grinding

Severe abrasive damage occurred in all the microstructures during grinding, demonstrated by a high surface roughness (Fig. 2). Observation of the ground surfaces and subsurfaces indicated that the material removal mechanism was affected by the three different microstructures. For EQ, the propagation and intersection of lateral cracks with the free surface and/or other crack systems caused the removal of large sections of material whose size was significantly greater than the grain size [EQ in Fig. 3(b)]. However, for EL, the material removal was associated with individual grain pull-out [EL in Fig. 3(b)] from the ground surface, only microcracking was observed in the subsurface [EL in Fig. 3(c)] In this present study, all the microstructures are of the same chemical composition. Therefore, different material removal processes are solely attributable to microstructural variables, i.e. grain size and aspect ratio.

During grinding, the shape of grinding particles can be classified as either sharp or blunt. As a result, subsurface damage observed in this work can be analysed via two relevant models: a sharp contact model[10] and a blunt contact model.[24,25] The sharp contact model deals with the formation of lateral cracks during sharp sliding contact (see Fig. 5), in which the length of a lateral crack, C_L, may be given[10,26] as:

$$C_L = \alpha\left[\frac{(E/H)^{3/5}}{K_{IC}^{1/2}H^{1/8}}\right]P^{5/8} \tag{1}$$

where α is a constant, E Young's modulus, H hardness, K_{Ic} fracture toughness and, P the applied load. Fracture toughness values given in Table 2 are from indentation fracture toughness measurements and are, hence, long-crack fracture toughness values. There has been prudent discussion in the literature[8] as to whether one should consider long or short-crack fracture toughness when analysing abrasion behaviour. A simplified generalisation may be that, when cracks are of the same order as the grain size, short-crack toughness is relevant; however, in the case of longer cracks, the cracks can be affected by crack extension toughening or R-curve behaviour, which results in a toughness increase that scales with crack length and microstructure.[27,28] The subsurface lateral cracks in EQ of Fig. 3(c) are larger than the grain size and hence it is necessary to consider the effect of microstructure upon the fracture toughness when applying Eq. (1) here.

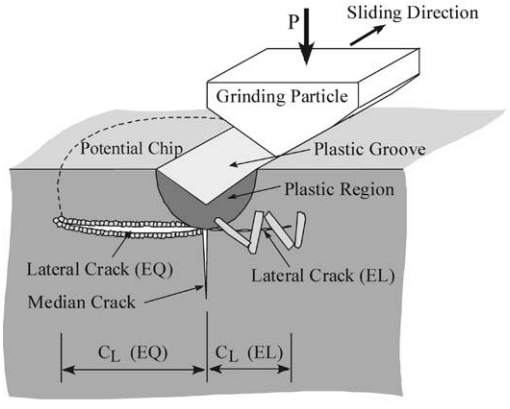

Fig. 5. Illustration of lateral crack propagation in EQ and EL during the sharp indenter sliding. Note that the large elongated grains reduce the lateral crack length.

Generally speaking, R-curve behaviour is a result of grain dislodgement leading to a bridging effect in the crack wake. To quantitatively describe how grain dislodgement is affected by grain size and morphology in ceramics, an analytical model was developed by Vekinis et al.[29] Here, we modify the model by assuming that the elongated grains are rod-like with the diameter $2a$ and the length L, thus, the aspect ratio $A_R = L/2a$. The work done to pull out each grain is given as:

$$\begin{aligned} W_g &= \int_0^{L/4} 2\pi a l\ \tau \mathrm{d}l \\ &= \frac{\pi}{4}\tau a^3 A_R^2 \end{aligned} \tag{2}$$

where τ is the average shear stress exerted by one grain against the matrix or another grain and is assumed to be constant, and l is the sliding distance of each grain before pulling out, averaged as $L/4$. The resulting increase in toughness, ΔR, can be formulated as:

$$\begin{aligned} \Delta R &= N_{bg} W_g \\ &= \frac{1}{4}\tau f a A_R^2 \end{aligned} \tag{3}$$

where N_{bg} is the number of bridging grains intercepting the crack plane, equal to $(f/\pi a^2)$, in which f represents the area fraction of bridging grains. It reveals that both grain size and, especially, aspect ratio have significant influence on the crack propagation resistance. The effective fracture toughness, K_R, of the material is a combination of the intrinsic fracture toughness, R_0, and the crack growth resistance, and given as:

$$K_R = \sqrt{E(R_0 + \Delta R)} \tag{4}$$

E and H are essentially the same for all these microstructures, and R_0 and τ would be expected to be similar as a result of identical material chemistry. Combining Eqs. (1), (3) and (4) gives:

$$C_L = \frac{kP^{5/8}}{\left(R_0 + \tau f a A_R^2\right)^{1/4}} \tag{5}$$

where k is an elastic/plastic material property constant and τ and f may be affected by microstructure. However,

Eq. (5) shows that lateral crack length can be reduced or suppressed by an increase in aspect ratio and, to a lesser extent, grain diameter. This result is in agreement with the observation that lateral and median cracks were seen in EQ, while such cracks were not seen in EL.

The blunt contact model is used to describe the criteria for the formation of microcracks and macrocracks. This model involves a conical ball pressed onto the surface, in which Hertzian cracks or 'quasi-plastic' zones that contain microcracks may form, depending upon the microstructure. It has been well established that, upon normal contact loading, a critical stress, P_Y, exists for the formation of a subsurface microcrack zone below the contact.[24] For some, as yet unexplained reason, this stress decreases with increasing grain size. Concurrently, another critical stress, P_C, exists for the formation of long cracks, analogous to the lateral and median cracks observed in EQ of Fig. 3(c). Should $P_Y < P_C$ then microcrack zones form prior to large cracks, as in EL. While for $P_C < P_Y$, large cracks preferentially form, as in EQ. This grain *size*–cracking behaviour relationship was also observed in Si_3N_4,[25] but no consideration was made of the effect of grain morphology.

In this current study microcracking is observed below the ground surface in EL [Fig. 3(b)], analogous to a contact load greater than P_Y, and it is proposed that these cracks did not further propagate due to enhanced toughening resulting from crack bridging by the elongated grains, as explained in Eq. (4). Subsurface microcrack lengths are expected to be in the order of the grain size. In the case of EQ, subsurface microcracking of this size could not be clearly resolved and was not observed. However, subsurface cracks, analogous to a contact load greater than P_C, are observed [e.g. Fig. 3(c)] and propagate due to low toughness in this material.

It can be concluded from the analyses of the two models above that large sections of material removal would occur during grinding of EQ following large lateral crack formation and propagation, but only grain-size material removal in EL.

4.2. Effect of microstructure on polishing

A significant improvement of surface quality took place after the samples were polished using 15 μm diamond paste, indicating that the material removal process underwent a transition from macro-scale to micro-scale. After the 1 μm diamond paste polishing, both EL and E/E showed the characteristics of even, mild material removal. However, EQ still exhibited extensive grain pull-out. As the chemistry of the materials is identical, the propensity of EQ to experience grain pullout appears to be related to the grain size and/or aspect ratio.

One may hypothesise that *no* grain pullout will occur when the energy to pull the grain out, i.e. the work of delamination of the grain within the 'matrix', W_{del}, plus the frictional work to pull the grain out, W_{po}, is greater than the energy to fracture the grain at the surface, W_f:

$$W_{del} + W_{po} > W_f \tag{6}$$

Considering the schematic representation shown in Fig. 6, the work of delamination may be taken as:

$$W_{del} = 4\gamma_i a\pi l \tag{7}$$

where γ_i is the specific fracture energy at the grain boundary and l the depth to which the grain is embedded below the surface.

The work of grain pullout may be taken as:

$$W_{po} = \tau\pi a l^2 \tag{8}$$

as per Eq. (2).

The energy to fracture the grain at the polishing surface may be taken as:

$$W_f = 2\gamma_g \frac{\pi a^2}{\sin\theta} \tag{9}$$

where γ_g is the specific surface energy of the grain and θ is the angle of incidence of grain to the surface. It is assumed that the long axis of the grain is not completely planar to the surface, i.e. $\theta > \sin^{-1}(1/A_R)$.

Assuming that the average grain is embedded half its length, $l = L/2$, one substitutes Eqs. (7)–(9) and $A_R = L/2a$ into (6) to derive the condition for a grain *not* to pull out as:

$$\frac{2\gamma_i}{\gamma_g} A_R + \frac{\tau a}{2\gamma_g} A_R^2 > \phi \tag{10}$$

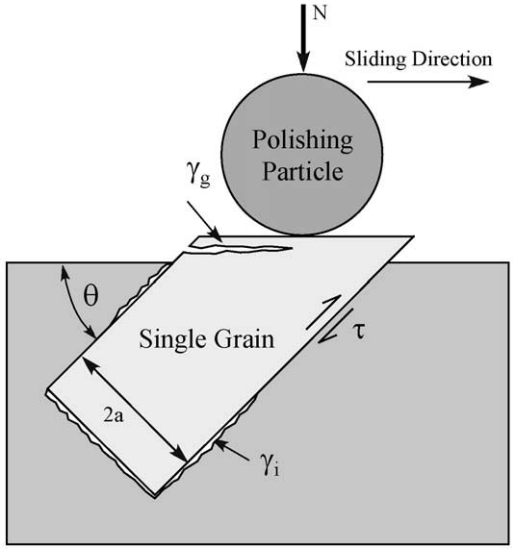

Fig. 6. Illustration of grain fracture versus grain delamination plus pullout during mechanical polishing.

where ϕ is a parameter which varies with the angle of incidence of the grain to the surface.

It can be seen that the grain aspect ratio has a strong influence on whether grain pull-out occurs. One can conclude that the possibility of grain pullout during polishing will be reduced by increasing the aspect ratio, the grain size, the interfacial bonding energy and by decreasing the fracture energy of the grain.

Eq. (10) may be assessed in terms of the material considered in this current study. Sun et al.[30] undertook an investigation of fracture behaviour of a range of Si_3N_4 ceramics, one of which exhibited similar characteristics to EL in this study; that is, an elongated grain aspect ratio of 6∼7 and a R-curve, which plateaued at $K_R \sim 7$ MPa$\sqrt{m}$. An investigation of crack growth in this material found that, when a crack encountered a grain lying at an angle of incidence greater than a critical value to the crack plane (60°), it followed the least energy path through the grain while at a smaller angle of incidence it progressed along the grain/matrix interface. From this observation, one may estimate that:

$$\gamma_i/\gamma_g \approx 1/\tan 60^\circ = 0.58 \quad (11)$$

for the materials in the present study. Micrographs from a fracture study of another Si_3N_4 material which exhibited very little R-curve behaviour show that fracture is essentially along the grain/matrix interface.[31] The same material had a fracture toughness of $K_c \sim 3.2$ MPa$\sqrt{m}$ which is similar to EQ in this study. As the chemistry of all materials in this study is the same, we assume that the interfacial fracture energy at the grain/matrix interface is the same. Noting that $2\gamma_i = K_c^2/E$ and taking Young's modulus as 320 GPa[32] and the indentation fracture toughness of EQ as the intrinsic fracture toughness, one obtains an estimate of fracture energy $\gamma_i = 21.39$ J/m^2, and from Eq. (11) $\gamma_g = 36.88$ J/m^2.

Measurements of crack closure stress in elongated grains bridging a crack in Si_3N_4/sialon material using Raman spectroscopy[33] may be used to estimate interfacial shear stress τ. At a distance ∼200 μm behind the crack tip, crack closure stress due to frictional effect in the bridging grains was measured as 124 MPa. The corresponding crack opening was 0.6 μm while the grain length, L, was 60 μm (diameter 6 μm), indicating that delamination had occurred, but very little grain pullout had taken place. Taking the average pullout length of a bridging grain on a fracture plane to be $\sim L/4$, one obtains a value of $\tau = 24.8$ MPa.

Substituting these values and the grain diameter ($2a$) of EL (0.7 μm) into Eq. (10) and taking an average angle of incidence $\theta = 45^\circ$ reveals that grain pullout will not occur for aspect ratios $A_R > \sim 1.1$. This may also be applied to elongated grains which are only partially embedded, i.e. $l/2a > 1.1$. Even accounting for possible errors in estimating the various variables in Eq. (10) and different grain orientations (i.e. different angles of incidence), it can be seen that the improved polishing behaviour of EL and E/E may be attributed to their elongated grain structure.

5. Conclusions

The following conclusions may be drawn from this present study:

(1) The aspect ratio plays a more important role in the influence of microstructure on the grinding and polishing behaviour.
(2) With the increase of the aspect ratio and grain diameter during grinding, the crack propagation and surface damage are suppressed.
(3) With the increase of the aspect ratio and grain diameter during polishing, the grain pull-out is reduced, and the surface quality is improved.

References

1. Chen, I.-W. and Rosenflanz, A., A tough Sialon ceramic based on α-Si_3N_4 with a whisker-like microstructure. *Nature*, 1997, **389**(6652), 701–704.
2. Wood, C. A., Zhao, H. and Cheng, Y.-B., Microstructural development of calcium α-sialon ceramics with elongated grains. *J. Am. Ceram. Soc.*, 1999, **82**(2), 421–448.
3. Xie, Z.-H., Hoffman, M. and Cheng, Y.-B., Microstructural tailoring and characterisation of a Ca α-sialon composition. *J. Am. Ceram. Soc.*, 2002, **85**(4), 812–818.
4. Allor, R. and Jahanmir, S., Current problems and future directions for ceramic machining. *Am. Ceram. Soc. Bull.*, 1996, **75**, 40–43.
5. Marshall, D. B., Lawn, B. R. and Cook, R. F., Microstructural effects on grinding of alumina and glass-ceramics. *J. Am. Ceram. Soc.*, 1987, **70**(6), C139–C140.
6. Cho, S. J., Hockey, B. J., Lawn, B. R. and Bennison, S. J., Grain-size and R-curve effects in the abrasive wear of alumina. *J. Am. Ceram. Soc.*, 1989, **72**(7), 1249–1252.
7. Xu, H. H. K., Padture, N. P. and Jahanmir, S., Effect of microstructure on material-removal mechanisms and damage tolerance in abrasive machining of silicon carbide. *J. Am. Ceram. Soc.*, 1995, **78**(9), 2443–2448.
8. Xu, H. H. K., Jahanmir, S., Ives, L. K., Job, L. S. and Ritchie, K. T., Short-crack toughness and abrasive machining of silicon nitride. *J. Am. Ceram. Soc.*, 1996, **79**(12), 3055–3064.
9. Mukhopadhyay, A. K., Chakraborty, D., Swain, M. V. and Mai, Y. W., Scratch deformation behavior of alumina under a sharp indenter. *J. Eur. Ceram. Soc.*, 1997, **17**, 91–100.
10. Evans, A. G. and Marshall, D. B., Wear mechanisms in ceramics. In *Fundamental of Friction and Wear of Materials*, ed. D. A. Rigney. American Society of Metals, Metals Park, OH, 1981, pp. 439–452.
11. Maksoud, T. M. A., Mokbel, A. A. and Morgan, J. E., Evaluation of surface and sub-surface cracks of ground ceramic. *J. Mater. Processing Tech.*, 1999, **88**, 222–243.
12. Desa, O. and Bahadur, S., Material removal and subsurface damage studies in dry and lubricated single-point scratch tests on alumina and silicon nitride. *Wear*, 1999, **225–229**, 1264–1275.

13. Braun, L. M., Bennison, S. J. and Lawn, B. R., Objective evaluation of short-crack toughness-curves using indentation flaw: case study on alumina-based ceramics. *J. Am. Ceram. Soc.*, 1992, **75**(11), 3049–3057.
14. Padture, N. P. and Lawn, B. R., Toughness properties of a silicon carbide with in situ-induced heterogeneous grain structure. *J. Am. Ceram. Soc.*, 1994, **77**(10), 2518–2522.
15. Xu, H. H. K. and Jahanmir, S., Effect of grain size on scratch damage and hardness of alumina. *J. Mater. Sci. Lett.*, 1995, **14**, 736–739.
16. Cook, S. G., Little, J. A. and King, J. E., Etching and microstructure of engineering ceramics. *Materials Characterisation*, 1995, **34**, 1–8.
17. Kara, H. and Roberts, S. G., Polishing behavior and surface quality of alumina and alumina/silicon carbide nanocomposites. *J. Am. Ceram. Soc.*, 2000, **83**(5), 1219–1225.
18. Anstis, G. R., Chantikul, P., Lawn, B. R. and Marshall, D. B., A critical evaluation of indentation techniques for measuring fracture toughness: I, direct crack measurements. *J. Am. Ceram. Soc.*, 1981, **64**(9), 533–538.
19. Lawn, B., *Fracture of Brittle Solids*. Cambridge University Press, 1993, pp. 230–241.
20. Swanson, P. L., Fairbanks, C. J., Lawn, B. R., Mai, Y. W. and Hockey, B. J., Crack-interface grain bridging as a fracture resistance mechanism in ceramics: I, experimental study on alumina. *J. Am. Ceram. Soc.*, 1987, **70**(4), 279–289.
21. Mai, Y. W. and Lawn, B. R., Crack-interface grain bridging as a fracture resistance mechanism in ceramics: II, theoretical fracture mechanics model. *J. Am. Ceram. Soc.*, 1987, **70**(4), 289–294.
22. Li, C. W., Lee, D. J. and Lui, S. C., R-Curve behaviour and strength for in-situ reinforced silicon nitrides with different microstructures. *J. Am. Ceram. Soc.*, 1992, **75**(7), 1777–1785.
23. (a) Rowlands, N. and Munroe, P., FIB for the evaluation of non-semiconductor materials. In *Proceedings of the 31st Annual Technical Meeting of the International Metallographic Society*, ed. D. O. Northwood, E. Abramovici, M. T. Shehata, and J. Wylie. ASM International, Materials Park, Ohio, USA, 1998, pp. 233–241; (b) Chaiwan, S., Hoffman, M., Munroe, P., Stiefel, U. Investigation of sub-surface damage during sliding wear of alumina using focused ion-beam milling. *Wear*, 2002, **252**(7–8), 531–539.
24. Lawn, B. R., Indentation of ceramics with spheres: a century after Hertz. *J. Am. Ceram. Soc.*, 1998, **81**(8), 1977–2071.
25. Lawn, B. R., Lee, S. K., Peterson, I. M. and Wuttiphan, S., Model of strength degradation from Hertzian contact damage in tough ceramics. *J. Am. Ceram. Soc.*, 1998, **81**(6), 1509–1529.
26. Marshall, D. B., Lawn, B. R. and Evans, A. G., Elastic/plastic indentation damage in ceramics: the lateral crack system. *J. Am. Ceram. Soc.*, 1982, **65**(11), 561–566.
27. Zenotchkine, M., Shuba, R., Kim, J. S. and Chen, I.-W., R-curve behavior of in situ toughened α-SiAlON ceramics. *J. Am. Ceram. Soc.*, 2001, **84**(4), 884–886.
28. Becher, P. F., Fuller, E. R. Jr. and Angelin, P., Matrix-grain-bridging contributions to the toughness of whisker-reinforced ceramics. *J. Am. Ceram. Soc.*, 1991, **74**(9), 2131–2135.
29. Vekinis, G., Ashby, M. F. and Beanmont, P. W. R., R-curve behaviour of Al_2O_3 ceramics. *Acta Metall. Mater.*, 1990, **38**(6), 1151–1162.
30. Sun, E., Becher, P. F., Plucknett, K. P., Hsueh, C. H., Alexander, K. B., Waters, S. B., Hirao, K. and Brito, M. E., Microstructural design of silicon nitride with improved fracture toughness: II, effects of yttria and alumina additives. *J. Am. Ceram. Soc.*, 1998, **81**(11), 2831–2840.
31. Becher, P., Sun, E., Plucknett, K., Alexander, K., Kang, E.-S., Hirao, K. and Brito, M., Microstructural design of silicon nitride with improved fracture toughness: I, effects of grain shape and size. *J. Am. Ceram. Soc.*, 1998, **81**(11), 2821–2830.
32. Barsoum, M. W., *Fundamentals of Ceramics*. McGraw-Hill, 1997.
33. Pezzotti, G., Muraki, N., Satou, K. and Nishida, T., In situ measurement of bridging stresses in toughening silicon nitride using Raman microprobe spectroscopy. *J. Am. Ceram. Soc.*, 1999, **82**(5), 1249–1256.